VOL. 19, NO. 5, MARCH 2024 ISSN 1819-6608
ARPN Journal of Engineering and Applied Sciences

www.arpnjournals.com

# NUMERICAL INVESTIGATION OF A DIESEL JET AT HIGH INJECTION PRESSURE - SEVERAL PARAMETRIC STUDIES

L. Souinida[1], M. Mouqallid[2] and A. En-Naji[1]
[1]Department of Physics, FST, Université Moulay Ismail, Errachidia, Morocco,
[2]Department of Energetics, ENSAM, Université Moulay Ismail, Meknes, Morocco
E-Mail: laidi_sou@yahoo.fr

**ABSTRACT**

The purpose of this work is to investigate the dynamic behaviour of a diesel spray. To this end, the calculation code used to simulate the spray is Fluent. The evolution of the jet is simulated using an averaged approach according to the Navier-Stokes equations. To complete the system of the averaged equations, we tested many turbulence models. The multiphase structure of the spray diesel is modelled within the Volume of Fluid (and its coupling with Level-Set models). The comparison of the penetration length of our numerical study by the experiment and by the calculation code AVBP gives a good agreement. Finally, we investigate the impact of several parameters (the ambient density, the diameter of the injection nozzle…) on the evolution of the diesel jet. The calculation results have contributed to an understanding of some physical phenomena governing the evolution of the diesel spray.

**Keywords:** numerical study, multiphasic flow, averaged approach, volume of fluid, fluent solver.

Manuscript Received 7 September 2023; Revised 10 March 2024; Published 30 April 2024

## 1. INTRODUCTION

The current development of diesel engines must respond to the need to reduce fuel consumption and comply with anti-pollution standards. This objective can only be achieved through a thorough understanding of the physical phenomena involved in engine functioning (cavitation, turbulence, atomisation, mixing, combustion, etc.). The injection of fuel into the combustion chamber is a spray that interacts with the surrounding air. The entrainment of hot air largely favours the vaporisation of the fine droplets in the spray and therefore influences the initial distribution of the fuel in vapour form. Controlling the mixture (fuel-air) in the combustion chamber is therefore essential to ensure optimal combustion [1].

Recently, the development of innovative combustion technologies in engines has accelerated. These efforts have led to the development of new concepts such as diesel engines with a common rail system, where the functioning of this complex system is only possible with perfect control of fuel combustion. Understanding the physical mechanisms involved in the mixture is therefore a major challenge for engine manufacturers.

To improve these new diesel engines, a detailed understanding of the physical phenomena involved is required, particularly during injection. Optical diagnostic methods are currently used to identify the flows encountered in these engines [2-5], but do not yet provide a detailed description. In particular, diesel sprays are optically very dense and it is still difficult to gain access to the zone close to the nozzle where the initial atomisation of the fuel takes place. This is all the more true since experimental spray analysis must be carried out under diesel engine operating conditions. Another way of analysing the physics and thus optimising direct injection diesel engines is through numerical simulation.

It provides access to the entire flow in the combustion chamber. There are different approaches to numerical simulation:

- DNS (Direct Numerical Simulation): This involves directly simulating the Navier-Stokes equations, without using any modelling. This is a very effective tool for understanding physical phenomena, as it provides very precise access to all the physical data. On the other hand, it requires a very high degree of spatial discretization and is therefore restricted, for the most part, to academic cases such as the studies by Ménard et al [6] and Salvador [7] for an injection velocity lower than that found in diesel engines. Therefore, this method cannot be used for diesel sprays at high injection pressure;
- LES (Large Eddy Simulation): This involves simulating only the large scales of the flow. This method requires modelling of the smallest scales, which is a little tricky in the case of two-phase and turbulent flows. Several studies using this approach have been carried out [8-11]. But, they require robust computing resources;
- RANS: the highly turbulent, multiphase character of the diesel spray makes it very tedious to study using the two previous approaches. Consequently, the use of the RANS approach is an alternative for the automotive industry. However, it requires a great effort in modelling.

It is this latter approach that we have used in this work. The aim is, firstly, to validate the numerical models with results from the literature and, secondly, to study the effect of physical parameters (ambient density, injection nozzle diameter…) on the evolution of the spray.

## 2. EQUATIONS

Using two Reynolds decompositions on the instantaneous Navier-Stokes equations for incompressible flow, we obtain averaged equations as follows:

- Continuity equation:

$$\frac{\partial u_i}{\partial x_i} = 0$$

- Momentum equations:

$$\frac{\partial u_i}{\partial t} + \frac{\partial u_i u_j}{\partial x_j} = -\frac{1}{\rho}\frac{\partial p}{\partial x_i} + \frac{\partial}{\partial x_j}\left[\vartheta\left(\frac{\partial u_i}{\partial x_j} + \frac{\partial u_j}{\partial x_i} - \frac{2}{3}\delta_{ij}\frac{\partial u_l}{\partial x_l}\right)\right] + F + \frac{\partial}{\partial x_j}\left(-\overline{u_i' u_j'}\right)$$

$u_i$ and $u_i'$ are, respectively, the main and fluctuating velocity components in the $x_i$ direction, $-\overline{u_i' u_j'}$ is the Reynolds stress tensor, p is the pressure, $\vartheta$ is the kinematic viscosity, $\rho$ is the fluid density, $\tau_{ij}$ is the strain rate tensor and F is the external forces in volume.

The term $\overline{u_i' u_j'}$ poses a closure problem for the system of averaged equations. It is composed of the correlation of the fluctuating velocity components describing the turbulence phenomenon. Thus, to close the system of equations, we need the turbulence models describing this term.

There are several categories of models in the Fluent solver:

- Turbulence model with one transport equation: The Spalart-Allmaras model [12];
- Two-equation turbulence models: variants of the k-ε, variants of the k-ω and the SAS (Scale Adaptive Simulation) ([13-18]);
- Turbulence model with 3 equations: the k-$k_L$- ω model [19];
- Turbulence model with 5 equations in 2D (7 equations in 3D): The RSM (Reynolds Stress Model) [20-21].

In the present work, we have used all the models mentioned above. After comparing and analysing the calculation results, we deduce the model or models that can best characterise the phenomenon of turbulence within the flow of a diesel spray.

To describe the multiphase nature of the flow, we have used the VOF and its coupling with the Level-Set, which are implemented in the Fluent. To follow the interface between the phases of the flow, we need an indicator function for each phase: this is the volume fraction $\alpha_k$ according to the following equation:

$$\frac{\partial \alpha_k}{\partial t} + U.\nabla\alpha_k = 0$$

Where U is the average velocity of the control volume and k is an index indicating each phase.

If we only consider the two-phase problem (which is our case), we only need to calculate a fraction of one phase to find the two fractions of each control volume taking into account that the sum is equal to 1.

## 3. GEOMETRY AND MESH

We decided to carry out the study in two dimensions because we were studying round cylindrical jets. Therefore, we used a rectangular geometry with a length of 20 cm and a width of 7 cm, intended for free-surface calculations. We drew edges inside the rectangle to refine the mesh in specific areas.

We tested three types of mesh (rectangular, triangular, and hybrid). After these tests, we opted for the triangular mesh, whose sensitivity to mesh size will be studied in the next section.

## 4. BOUNDARY CONDITIONS

They play an important role in determining the solution to any fluid flow problem. Various fluid mechanics problems are governed by the same equations, but the boundary conditions can distinguish them. In this study, we have defined two conditions of boundaries: “pressure outlet” and “velocity inlet”.

For the injection of a diesel jet into a free surface, we have defined the “pressure outlet” condition at the boundaries of the calculation zone (except for the jet outlet), where the pressure and temperature are equal to those of the ambient environment.

### Jet Exit

In the discharge section, the parameters that can be defined are, on the one hand, the injection velocity (velocity inlet) and, on the other hand, the volume fraction of a liquid. In the present work, we always set the volume fraction of the liquid at the nozzle outlet equal to 100% (in line with experimental data [22]). We also define "velocity inlet" as the boundary condition. But sometimes we have a variable velocity as a function of time after injection and other times constant. We programmed the time-varying velocity profile using the 'C' language and implemented it in the Fluent solver.

For the simulation of the evolution of the spray on a free surface, the conditions we have defined at the jet exit are those of Verhoeven *et al* [22]. The profile of the velocity at the jet exit (Figure-1) is the one used by Martinez [23] and Beau [24]. It corresponds to the flow velocity obtained from Verhoeven *et al* [22] mass flow measurements. To validate the model used in this work, we considered that the direction of the exit velocity is normal to the flowing section. The density of the liquid is$\rho_l = 780\ \mathrm{kg.m^{-3}}$, and its absolute temperature is T = 360 K. The temperature in the chamber is T=387 K and the diameter of the injection nozzle is d=0.2 mm.

Concerning the jet exit velocity, the liquid introduction rate measured by Verhoeven *et al* [22] is very unsteady. Nevertheless, we can distinguish three main periods. The first corresponds to the start of the injection with a rapid increase in the introduction rate. It then increases progressively. Finally, it decreases during the needle closure period.

To take account of these instabilities, we proceeded, in the same way as Beau [24], as follows:

- For the first phase, we assume that the flow rate varies linearly until the second phase. The time taken for this phase determines the time slope of the first injection period;
- In the second phase, we assume that the flow rate increases linearly, using the same slope as Beau [24] ;
- For the third phase, we proceed in the same way as in the first, with a decreasing rate of introduction.

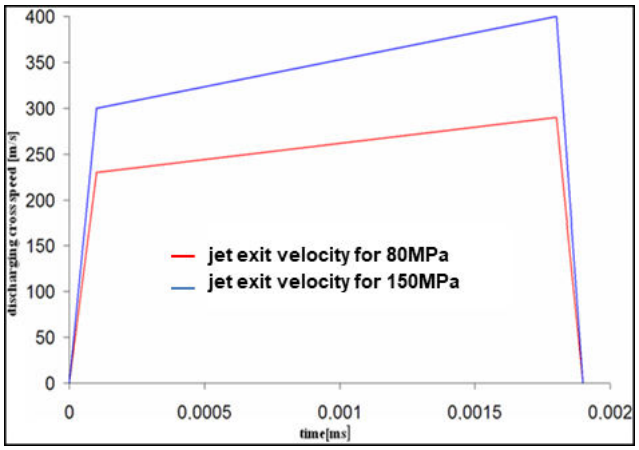


**Figure-1.** Velocity upon time at jet exit [24] deduced from measured injection flow rate profile [22].

To study the effect of nozzle diameter on spray evolution, we based ourselves on the study by Martinez-Martinez *et al* [25] for all injection and ambient conditions (Tables 1 and 2). We used the high-pressure injection value of $P_i = 130\text{MPa}$ for three injection nozzle diameters (d=0.13 mm, d=0.17 mm, and d=0.2 mm) in the present study.

**Table-1.** Injection and ambient conditions.

| Nozzle diameter (µm) | 130 – 170 – 200 |
|---|---|
| Injection pressure (MPa) | 130 |
| Ambient temperature (°C) | 70 |
| Ambient pressure (MPa) | 0.13 |

**Table-2.** Injection parameters and their corresponding discharge coefficients.

| Injection pressure (MPa) | Nozzle diameter (µm) | Discharge coefficient $C_d$ |
|---|---|---|
| 130 | 130 | 0.733 |
| 130 | 170 | 0.666 |
| 130 | 200 | 0.651 |

## 5. RESULTS AND DISCUSSIONS

We will present the results of our numerical study, using an averaged approach, of the dynamic behaviour of a diesel spray at high injection pressure. These results will concentrate on the impact of the geometric and physical parameters influencing the evolution of the diesel spray. In the first section, we will analyse the comparison of our calculations with literature results to validate the turbulence models, the numerical schemes, and the two-phase models used in the present study. The effect of ambient conditions (ambient gas density) on the characteristic quantities of the diesel jet will be discussed in the second section. In the third section, we will study the effect of injection pressure ($P_i = 80$ MPa, $P_i = 150$ MPa) on the evolution of the diesel spray. The effects of the parameters at the outlet of the injection nozzle (turbulent intensity and diameter of the injection nozzle) will be dealt with in the fourth and fifth sections.

### 5.1 Comparing Turbulence Models

To highlight the results of the simulations, we opted to compare the temporal evolution of the penetration length as a quantitative validation criterion. To this end, we plotted the simulation curves against those of the experiment and those of the filtered calculation. In addition, we visualised images of the simulation in comparison with previous results for a qualitative comparison.

#### 5.1.1 Spray morphology

The liquid volume fraction field is an important parameter in the modelling of two-phase flows. In the case of diesel sprays, it gives us information about the morphology of the jet and the dispersion of the liquid in the gas (the fuel-air mixture). In Figure-2, we have visualised the liquid volume fraction field for two instants after injection, namely: $t_1 = 0.3$ ms and $t_2 = 1$ ms, for an injection pressure ($P_i = 80\text{MPa}$) and ambient density ($\rho_a = 25\ \text{kg.m}^{-3}$).

In the same figure, we compare the different turbulence models. The simulation images of all the turbulence models show, on the one hand, a symmetrical penetration of the diesel spray into the ambient air and, on the other hand, a widening at the front of the spray.

However, for calculations using the models (Spalart Allmaras, k-ε, k-ω, SAS), the images show faster penetration than those corresponding to the k-$k_L$-ω and RSM models. Apart from the jet front, the jet diameter of the four models in the axial positions is very small compared to that of the k-$k_L$-ω and RSM models. We can explain these differences based on the degree of absorption of the liquid by the ambient air, fractionating the liquid more and influencing the aerodynamic effects thus blocking the spray from penetrating the ambient environment [26].

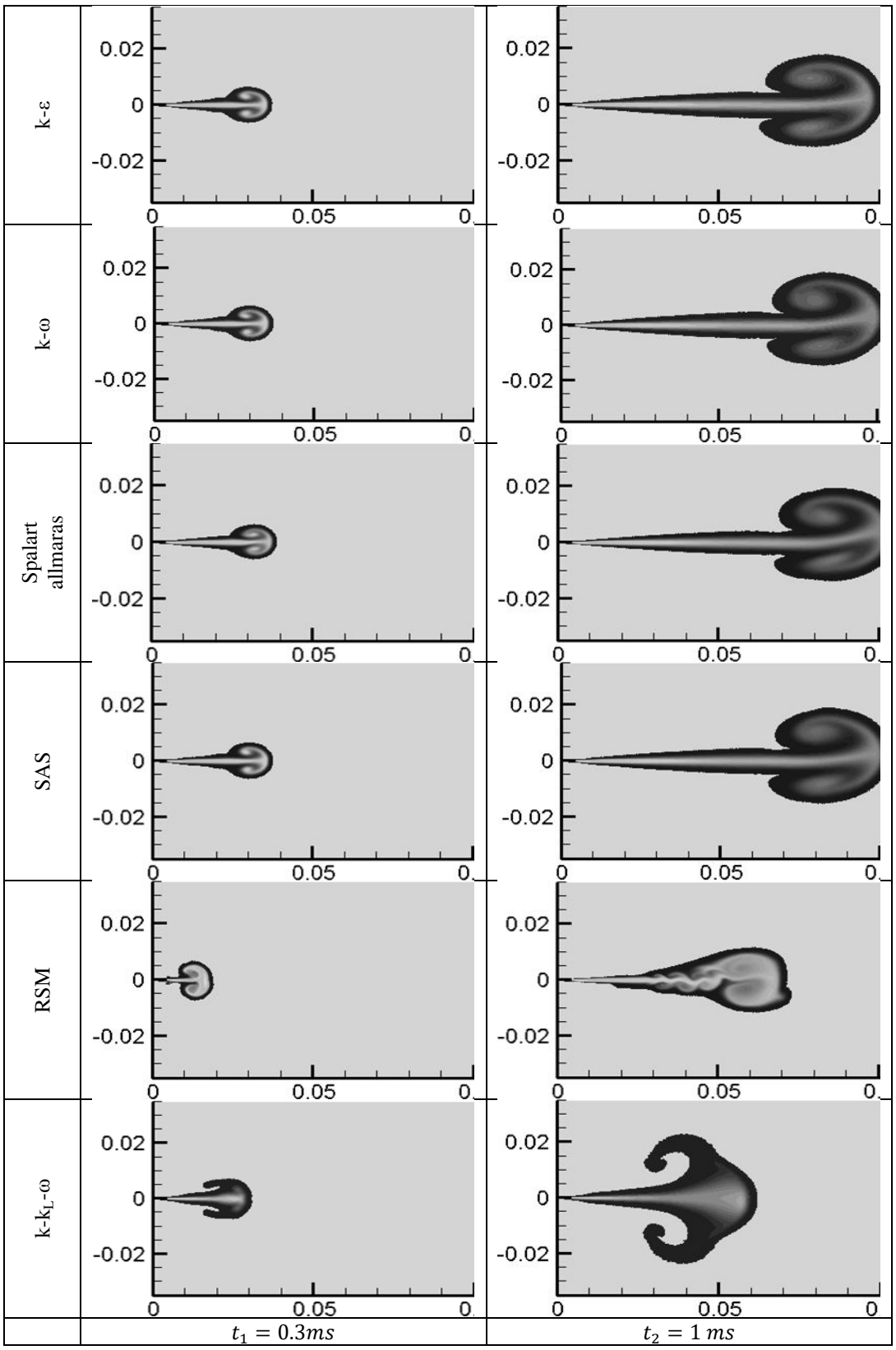


**Figure-2.** Liquid volume fraction field (jet morphology): $P_i = 80$ MPa , $\rho_a = 25$ kg. $m^{-3}$.

**5.1.2 Potential core of the spray**

The liquid core or potential core is the part of the jet very close to the injection nozzle, which is very dense in the liquid. It is highlighted, firstly by the volume fraction of the liquid, which must be very close to 1, and secondly by its length through the average velocity of the mixture. This length is the distance where the average velocity curve remains constant along the axis of the jet

and is equal to the velocity at the outlet of the injection nozzle.

The liquid core is a very important parameter to study numerically and to model in diesel sprays. This importance stems from the difficulties encountered on an experimental scale [27]. Optical measurement techniques are unable to detect it. Therefore, methods based on the electrical conductivity of the liquid are used and are easier to develop. However, the accuracy of these measurements is very low [28].

**The average velocity of the mixture**

In Figure-3, we present the curves of the mean velocity of the mixture on the jet axis ($y = 0$) at a given instant during injection ($t = 0.6$ ms) for all the turbulence models mentioned above. The simulation curves corresponding to k-ω SST, k-ε and SAS show that from $x = 0$ to $x \cong 15\,d$, the average velocity stays constant along the jet axis, after this distance the velocity starts to decrease slightly. This result shows that the potential core can have a length of the order of $L_{no} = 15\,d$ which is relatively large compared to literature results [26].

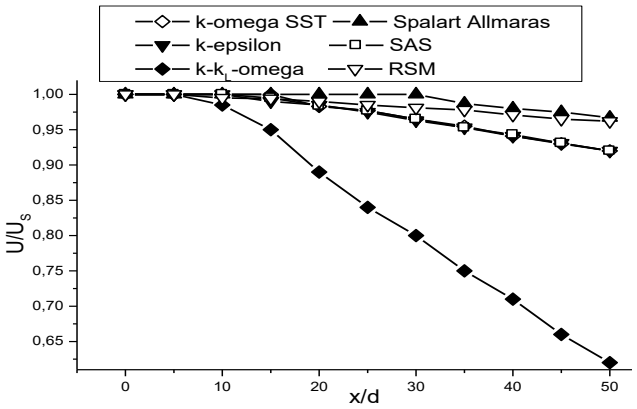


**Figure-3.** The average velocity of the mixture on $y = 0$ at $t = 0.6$ ms.

For the curve according to the Spalart allmaras, the velocity remains constant up to $x \cong 28\,d$. This may inform us that the length of the potential core is of the order of $L_{no} = 28\,d$, which is an overestimate compared to the literature results.

As far as the RSM model is concerned this length is of the order of $L_{no} = 5\,d$. We can also see that after this distance the mean velocity along the axis of the jet decreases very slowly.

Finally, for the k-$k_L$-ω model, the length of the potential core is of the order of $L_{no} = 10\,d$. After this distance, the average velocity along the axis of the jet decreases very rapidly. This can be explained by the increase in liquid-gas interfaces, which generate significant aerodynamic forces.

**5.1.3 Penetration length**

In Figure-4, we have plotted the penetration length upon time of the diesel spray of $P_i = 80$ MPa and $\rho_a = 25\,\mathrm{kg.m^{-3}}$, for the turbulence models mentioned previously. The simulation results are compared with those from Verhoeven [22] and Martinez [23], to select the model that best characterises the behaviour of the diesel spray at high pressure [26].

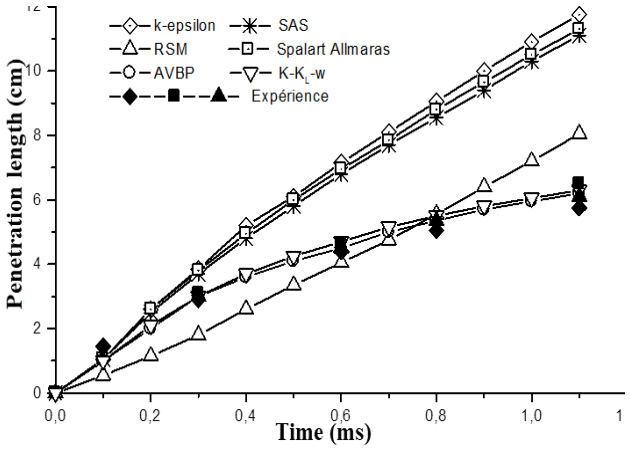


**Figure-4.** Penetration length upon time: $P_i = 80$ Pa, $\rho_a = 25\,\mathrm{kg.m^{-3}}$[26].

After analysing the several turbulence models used to complete the system of averaged equations to study the behaviour of the diesel spray dynamics in terms of the diesel spray penetration length [26], we can deduce that k-$k_L$-ω is the model that may be valid in our work [26].

**5.1.4 Sensitivity of selected models to injection pressure**

Engine manufacturers always think in terms of high injection pressures to ensure good atomisation of the fuel. In practice, they use very sophisticated injection systems (Common Rail). To respond numerically to this trend, we carried out the calculation by increasing the injection pressure.

In Figure-5, we have plotted the penetration length upon time of the diesel jet for an injection pressure $P_i = 150$ MPa and an ambient density $\rho_a = 25\,\mathrm{kg.m^{-3}}$, adopting the models (k-$k_L$-ω; VOF). The simulation curves are compared with those of Verhoeven [22] and Martinez [23].

The simulation curve of our calculation agrees with the filtered calculation of Martinez [23]. The simulation curves agree with the experimental results of Verhoeven *et al* [22] after the instant $t = 0.2$ ms from the start of injection. The difference that existed before this time (the experimental tests give a large penetration compared with the calculation) can be explained by the choice of velocity profile at the outlet of the injection nozzle, which assumes that the discharge section is equal to the geometric section.

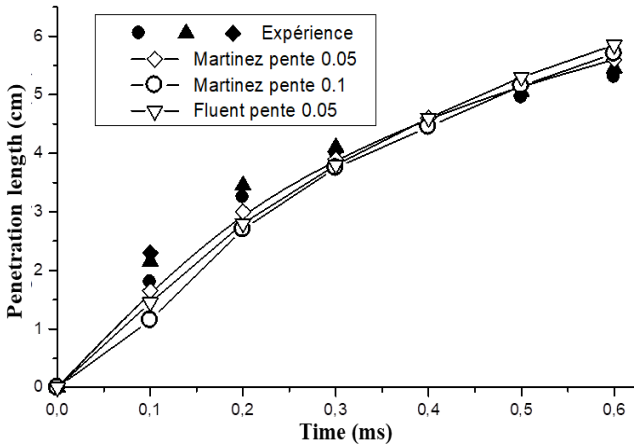


**Figure-5.** Penetration length upon time: $P_i = 150MPa$ , $\rho_a = 25\ kg.m^{-3}$.

### 5.1.5 Field of the average velocity of the mixture

The experimental tools used to measure the mean velocity of the diesel spray (optical in general) are very tricky to implement, given the high velocity of the flow and the high density of the liquid near the outlet of the jet. They are also unable to give the full field of the average velocity of the spray. On the other hand, the numerical simulation can visualise this field throughout the calculation domain at each instant, particularly in the zones where the liquid is located.

In Figures 6 and 7, we present the average velocity of the mixture in the zones where the liquid is located (liquid volume fraction $10^{-7} < \alpha_l < 1$) for different instants after injection ($t = 0.2$ ms ; $t = 0.4$ ms ; $t = 0.6$ ms ; $t = 0.8$ ms ; $t = 1$ ms ; $t = 1.2$ ms) for two injection pressures ($P_i = 80MPa$, $P_i = 150MPa$) and an ambient density $\rho_a = 25\ kg.m^{-3}$.

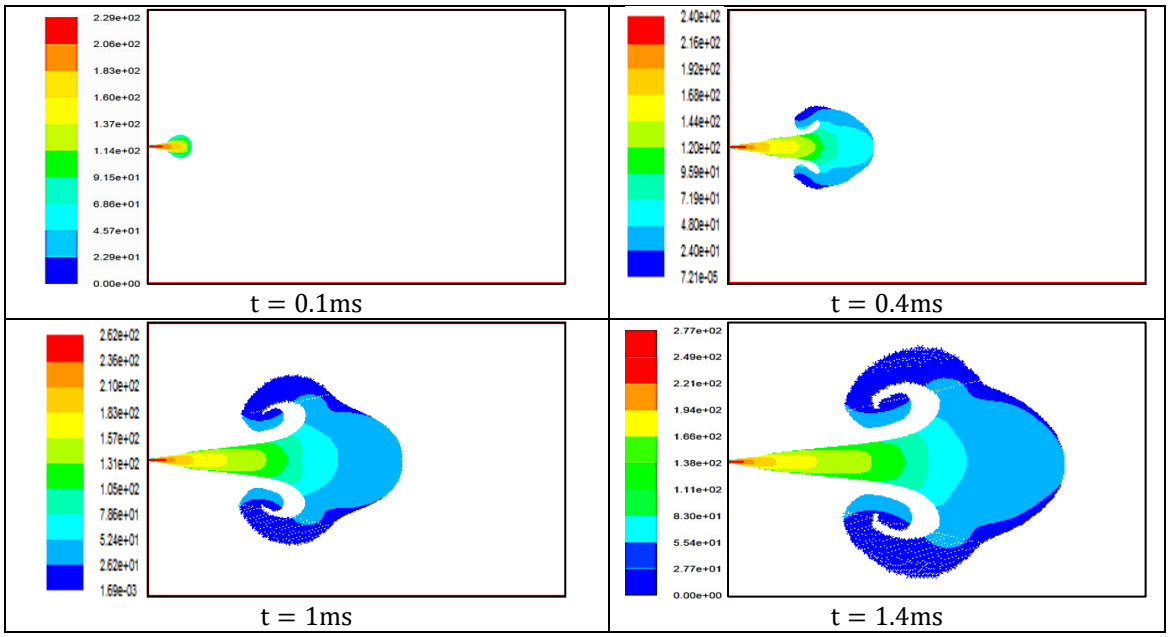


**Figure-6.** Field of the average velocity of the mixture: $P_i = 80MPa$ et $\rho_a = 25\ kg.m^{-3}$.

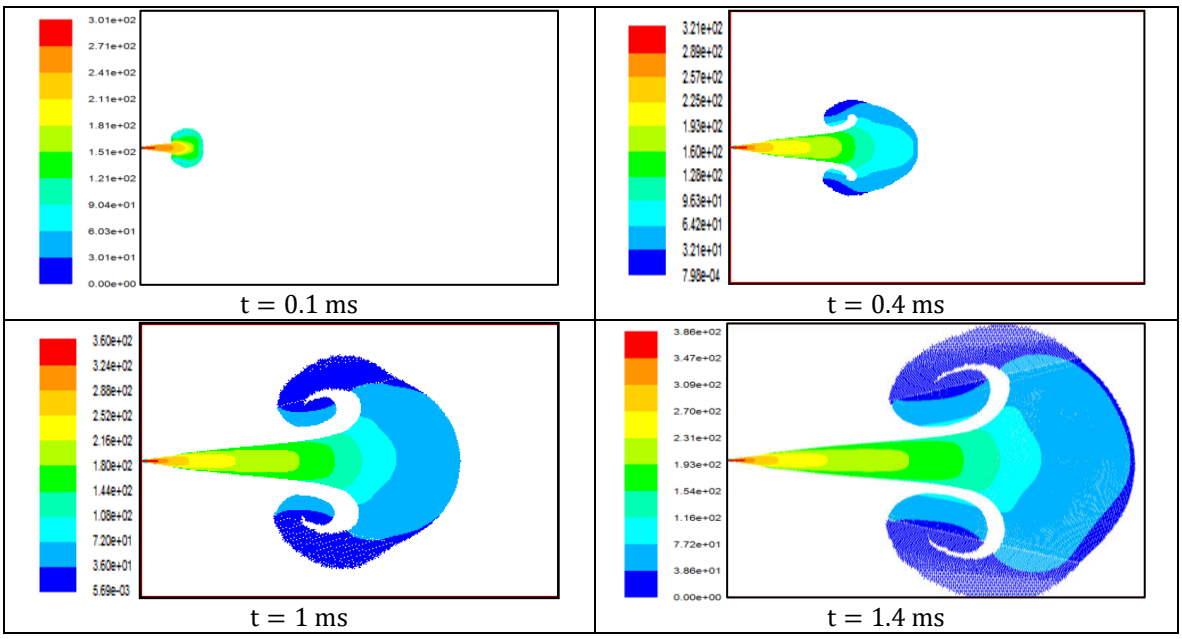


**Figure-7.** Field of the average velocity of the mixture: $P_i = 150\text{MPa}$, $\rho_a = 25\ \text{kg.m}^{-3}$.

The simulation images in the two figures show a symmetrical evolution of the spray and also show the widening as a function of time after injection. This symmetry is noticeable both in the shape of the spray and in the iso-surfaces of the average velocity field of the mixture.

**Summary**

In this paragraph, we have visualised results found using several turbulence and two-phase models for $P_i = 80\text{MPa}$. The models that give results in agreement with the literature are the k-$k_L$-ω turbulence model and the VOF and CLSVOF two-phase models. Again using the same models validated at $P_i = 80\text{MPa}$, but changing the injection pressure to $P_i = 150\text{MPa}$, we find that the simulation calculation results are still in agreement with the literature.

**5.2 Sensitivity to Numerical Schemes and Coupling Algorithms**

This paragraph is intended, on the one hand, to study the sensitivity of the space-time numerical schemes to the parameters to be solved and, on the other hand, to study the sensitivity to the coupling algorithms (pressure-velocity). This study is carried out using the same models validated in the previous paragraph.

**5.2.1 Spatial discretisation schemes**

**5.2.1.1 Volume fraction schemes**

In Figure-8, we present the liquid volume fraction field for different spatial discretization schemes of the liquid volume fraction advection equation. The simulation image that gives the correct shape of the diesel jet is the one corresponding to the "First order upwing" spatial discretisation scheme for the liquid volume fraction.

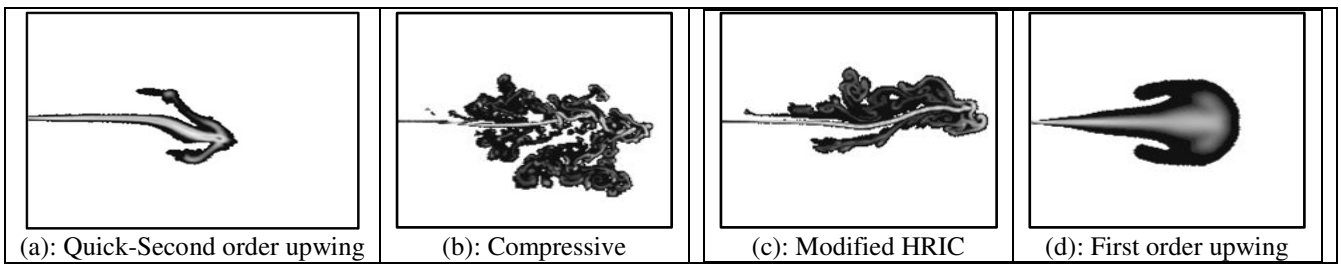


**Figure-8.** Liquid volume fraction field: sensitivity to volume fraction schemes.

**5.2.1.2 Pressure schemes**

The liquid volume fraction field is highlighted in Figure-9 for two pressure discretisation schemes: the "PRESTO" scheme and the "Body Force Weighted" scheme. The simulation images corresponding to the "PRESTO" show jet asymmetry after $t = 0.2$ ms. On the other hand, when we use the "Body Force Weighted" scheme, the jet retains its symmetry. We can say that this last scheme is valid, as its name indicates when we have important volume forces (aerodynamic effects in the context of this study).

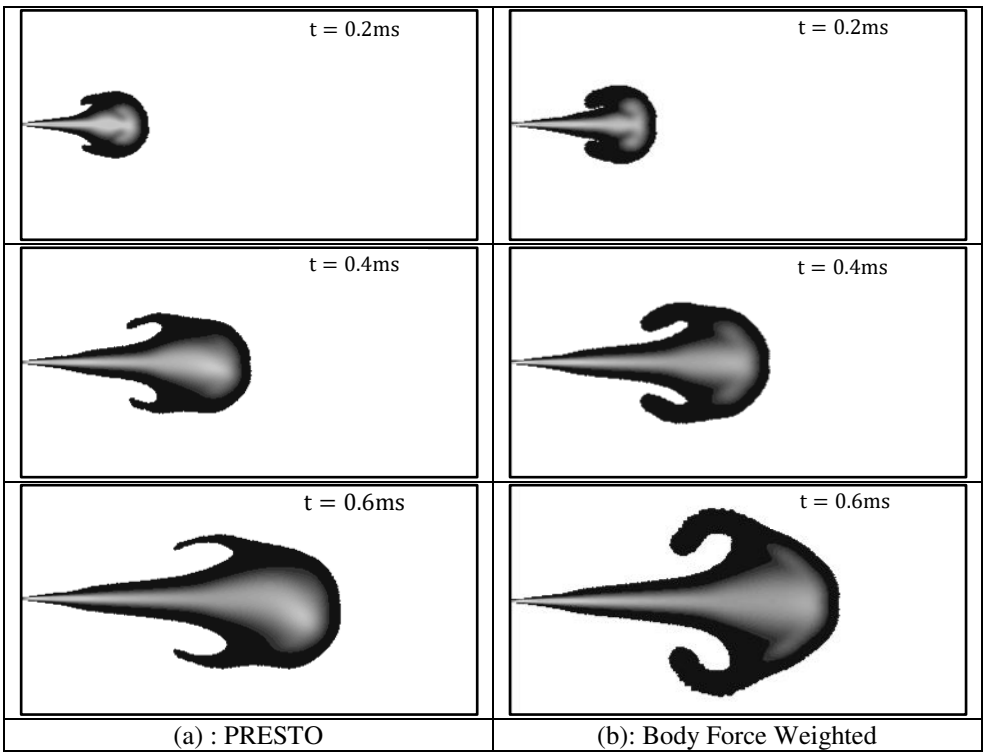


**Figure-9.** Liquid volume fraction field for two pressure schemes.

**5.2.1.3 Schemes of the momentum equation**

Figure-10 shows the liquid volume fraction field for five spatial discretization schemes of the momentum equation. We can see from the simulation images corresponding to the "Power Low", "Quick" and Third Order MUSCL schemes that the jet is non-symmetrical and blocked. On the other hand, when we use the "First order upwing" and "Second order upwing" schemes (used for the calculation validated by the literature), we can see the correct morphology of the jet. However, the "First order upwing" scheme underestimates penetration. We can deduce from the results of these four schemes that the "Second order upwing" scheme is the most suitable for the present numerical calculation.

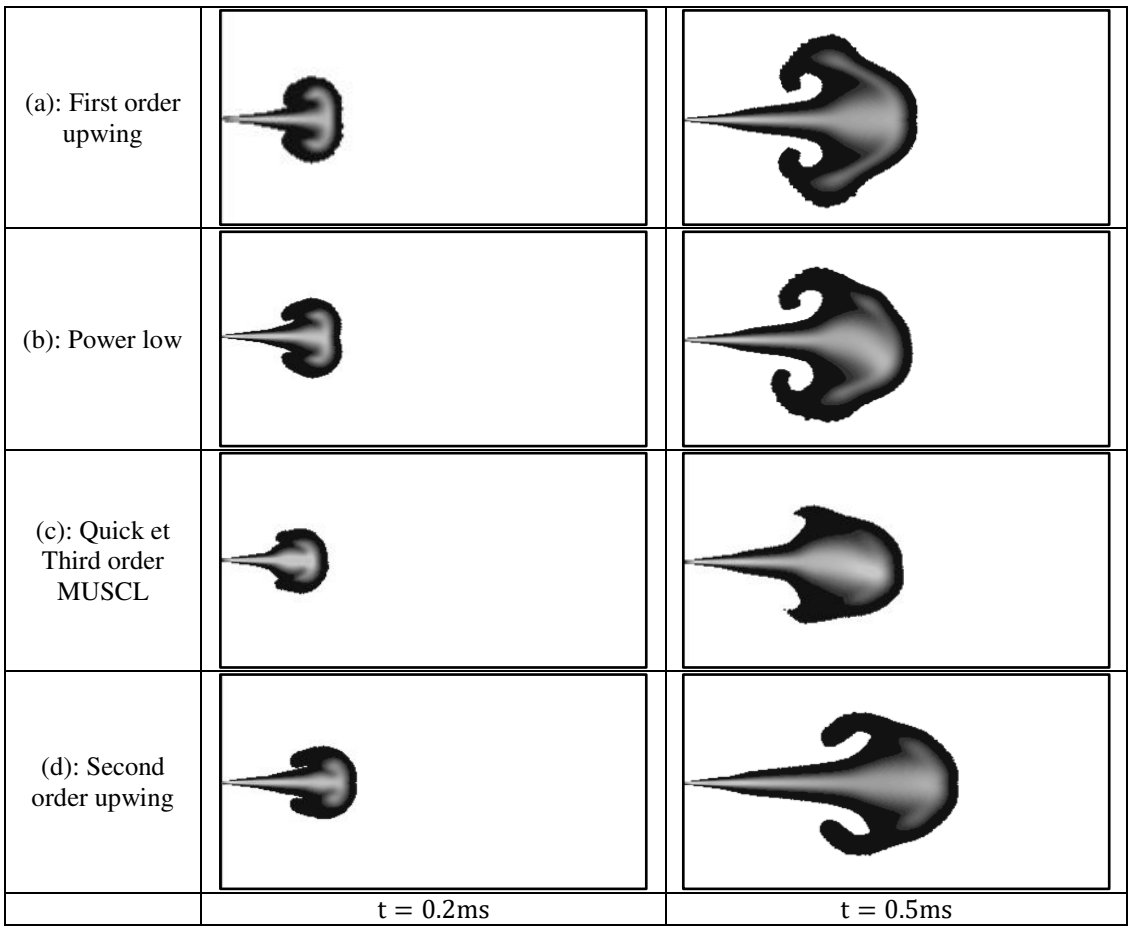


**Figure-10.** Liquid volume fraction field for different momentum equation schemes.

#### 5.2.1.4 Schemes of the scalar equations of the turbulence model

In Figure-11, we visualise the liquid volume fraction field for the scalar turbulence quantities: turbulence kinetic energy and laminar kinetic energy using two discretisation schemes while fixing the "First order upwing" scheme for the specific dissipation rate. We tested the "Second order upwing" scheme for this last parameter, but the calculation diverges. We can deduce that the scheme that should be used for these turbulence quantities is the "First order upwing" scheme.

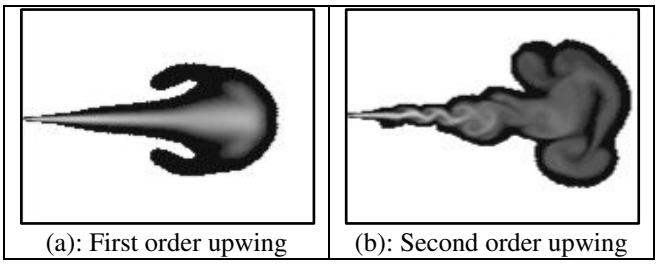


**Figure-11.** Liquid volume fraction field for two spatial schemes of laminar and turbulent kinetic energy equations.

#### 5.2.2 Temporal discretisation schemes

The liquid volume fraction field is shown in Figure-12 for three time-discretization schemes. The schemes which give a symmetrical and conical morphology are: "First order implicit" and "Bounded second order implicit". However, the "First order upwing" scheme underestimates spray penetration (we used the "Bounded second order implicit" scheme to validate the calculation results in the first paragraph).

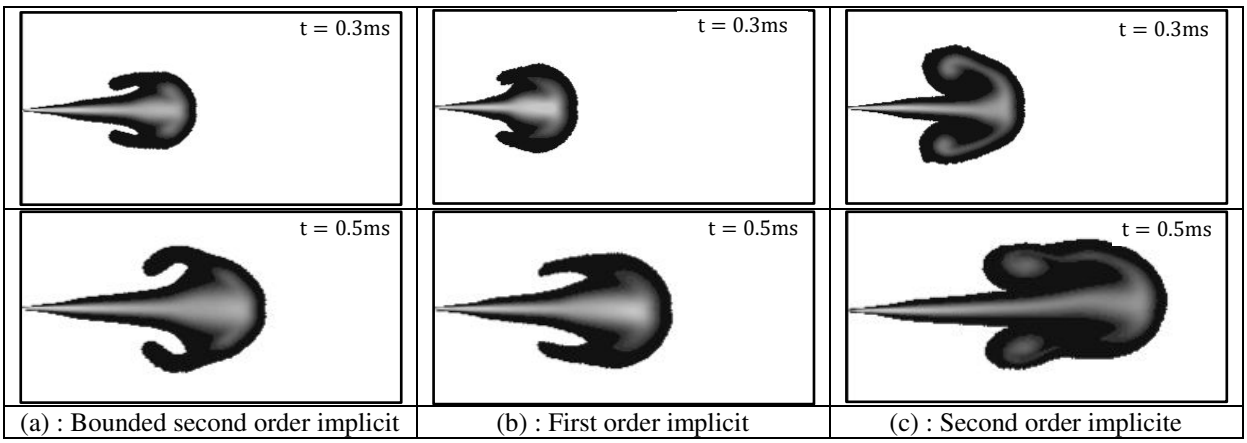


**Figure-12.** Liquid volume fraction field: sensitivities to time-discretisation schemes.

### 5.2.3 Coupling algorithms

Figure-13 represents the liquid volume fraction field for different pressure-velocity coupling algorithms ((a): the "SIMPLE" algorithm, (b): the "Coupled" algorithm, (c): the "PISO" algorithm). The image taken at $t = 0.6$ ms for the SIMPLE algorithm shows a slight jet asymmetry. On the other hand, the images corresponding to the other two algorithms show a correct Spray morphology. However, the Coupled algorithm overestimates spray penetration.

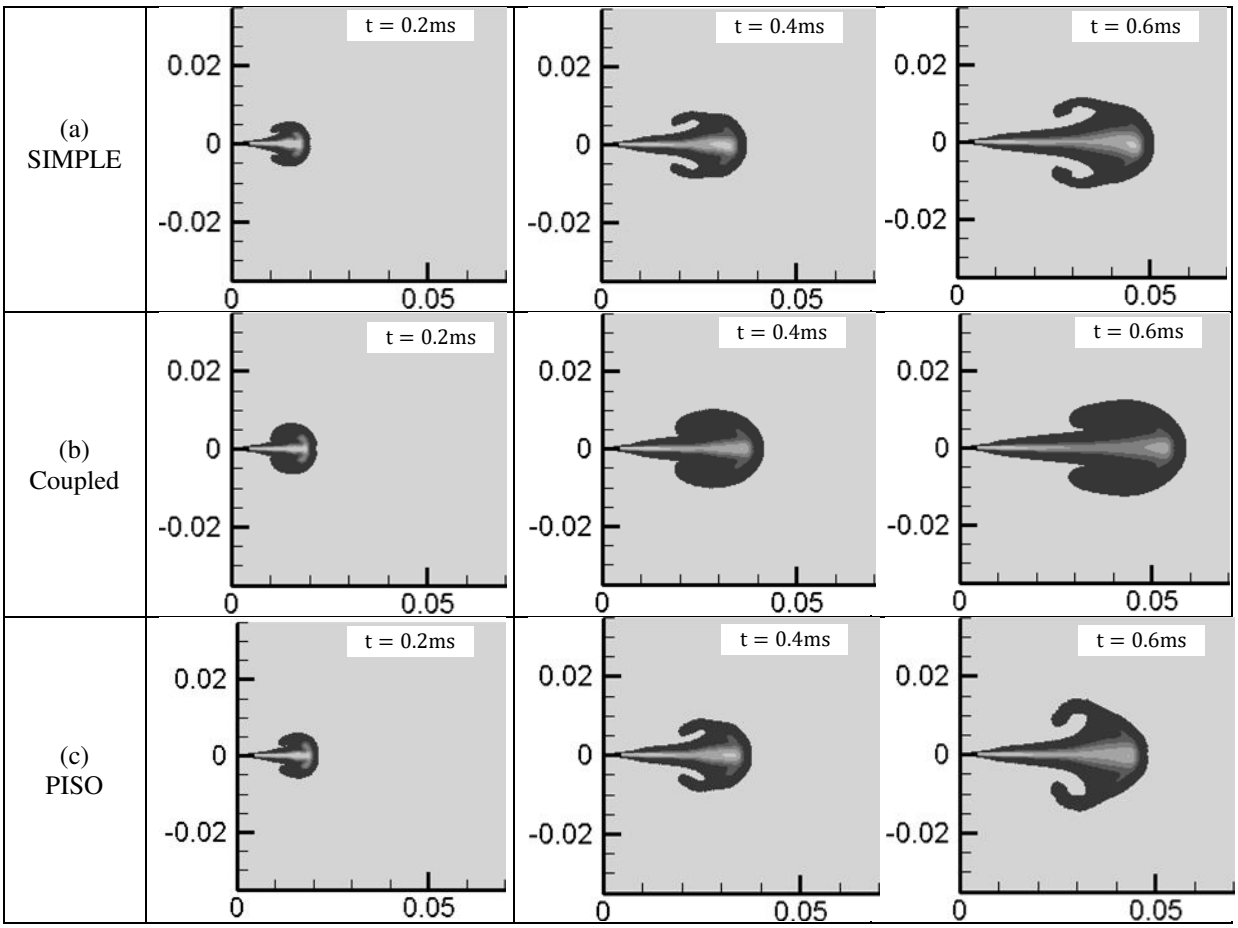


**Figure-13.** Volume fraction field for three coupling algorithms.

We can therefore deduce that the pressure-velocity coupling algorithm best suited to calculating diesel sprays is the PISO algorithm.

**Summary**

In this paragraph, we have presented results found using several space-time numerical schemes and several coupling algorithms between hydrodynamic variables. The simulation calculations were carried out

using the same models and conditions as previously validated. The following table summarises the numerical schemes and the coupling algorithm used for the simulation calculation results obtained throughout the work carried out as part of this study:

**Table-3.** Numerical schemes and coupling algorithms are valid for our work.

| **Coupling algorithm** | | **PISO** |
|---|---|---|
| Numerical spatial schemes | **Pressure** | **Body Force Weighted** |
| | Velocity | Second order upwing |
| | Liquid volume fraction | First order upwing |
| | Energy | Second order upwing |
| | Turbulent kinetic energy | First order upwing |
| | Laminar kinetic energy | First order upwing |
| | Specific dissipation rate | First order upwing |
| Numerical time scheme | | Bounded second-order implicit |

### 5.3 Mesh Sensitivity

After specifying the models and schemes to be used in this work, we studied the sensitivity of the calculation to the mesh size by adopting two parameters: the volume fraction of the liquid, which highlighted the total morphology of the jet, and the penetration length.

Figure-14 shows the liquid volume fraction field for three meshes: coarse (231987 cells), reference (371979 cells), and refined (449668 cells). The reference mesh is the mesh we used to validate the computational results with the literature in the first paragraph. The simulation images show a similarity (a conical shape and symmetry concerning the jet axis) between the results of the different meshes, except for a slight asymmetry of the jet in the third image concerning the refined mesh.

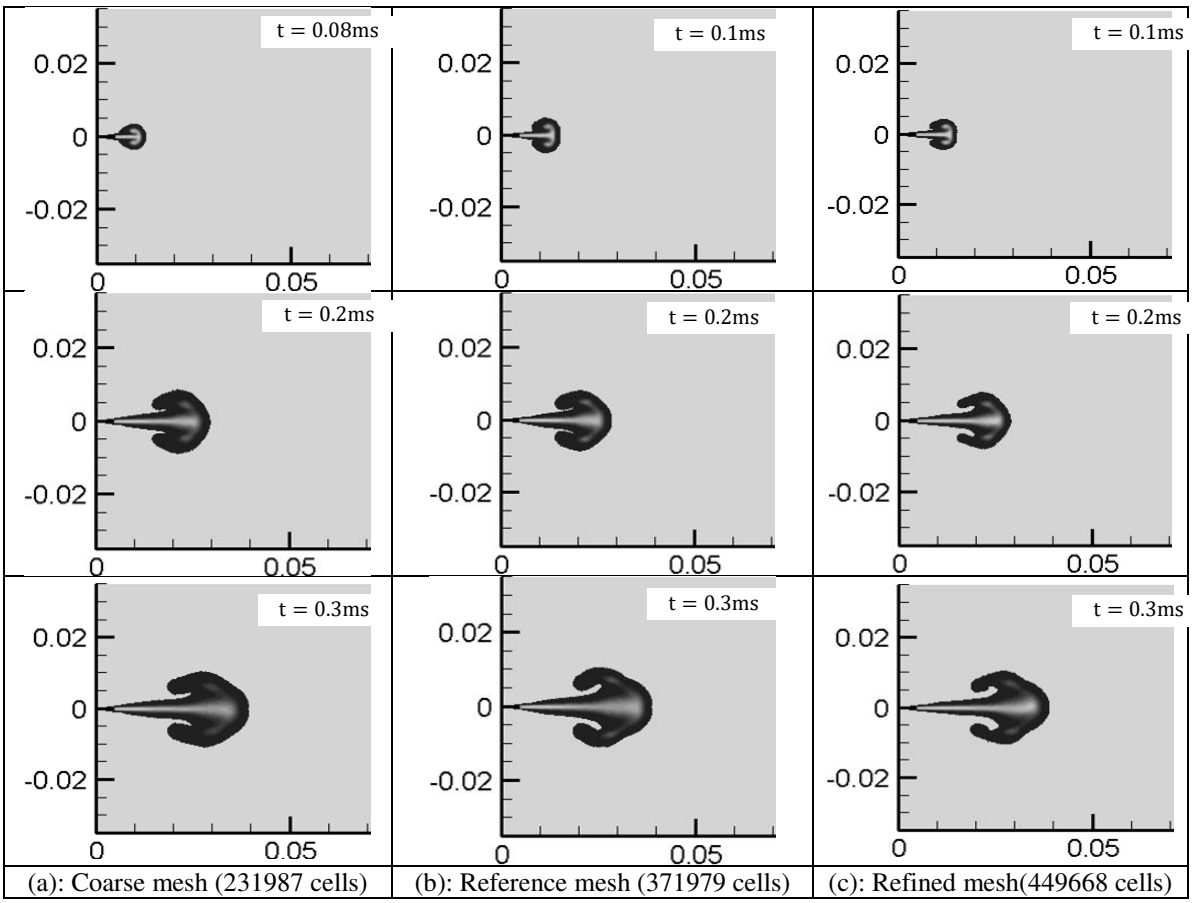


**Figure-14.** Evolution of the Spray over time for three mesh sizes.

Using the simulation images, we measured the jet penetration length for the three meshes (Figure-15). The curves show that the calculations for the refined case and the reference case coincide. However, for a coarse mesh, we can see a faster penetration from $t = 0.2$ ms after injection.

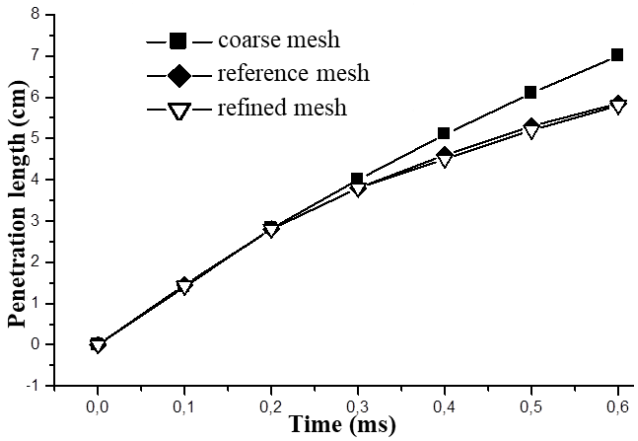


**Figure-15.** Penetration length upon time: Mesh sensitivity.

We can deduce from the above results that we need to stay within a given interval of mesh sizes used in this study to have a correct jet morphology and penetration that follows that of the experiment. The reference mesh used in this study falls within this interval.

### 5.4 The Effect of Ambient Density and Injection Pressure on Spray Evolution

#### 5.4.1 Impact on penetration length

In Figure-16, we have plotted the penetration length upon time of the diesel jet for two injection pressures and three ambient densities ($\rho_a = 15\ \mathrm{kg.m^{-3}}$, $\rho_a = 25\ \mathrm{kg.m^{-3}}$et $\rho_a = 35\ \mathrm{kg.m^{-3}}$). We can see that as the density of the ambient air increases, the penetration length of the spray decreases. Also, the two curves corresponding to $\rho_a = 25\ \mathrm{kg.m^{-3}}$ and $\rho_a = 35\ \mathrm{kg.m^{-3}}$ indicate that there are two phases in the evolution of the penetration length. In the first (from $t = 0$ ms to $t = 0.25$ ms), penetration is rapid, and after $t = 0.25$ ms, it becomes slow. However, for the two curves corresponding to $\rho_a = 15\ \mathrm{kg.m^{-3}}$, the two phases of the penetration are not noticeable for the two injection pressures.

This reduction in penetration length can be explained by the increase in aerodynamic effects, which are proportional to the density of the ambient air. However, for these forces to have a significant effect, giving rise to the second phase of penetration mentioned above, the density of the gaseous environment must exceed a certain limit.

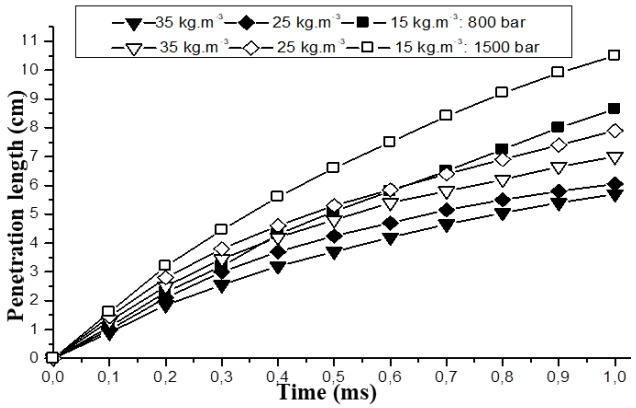


**Figure-16.** Penetration length upon time.

If we fix the ambient density, the simulation curves for the injection pressure $P_i = 150$MPa show rapid penetration compared to that using the pressure$P_i = 80$MPa. We can therefore deduce that the pressure at the jet outlet has a major effect on spray penetration. The injection pressure is linked to the inertia it gives to the liquid to penetrate the gas.

#### 5.4.2 Effect on cone angle

The spray cone angle tells us about the processes that occur in spraying, such as atomisation and air entrainment. Indeed, it is closely linked to the overall behaviour of the spray, and in particular its penetration. However, it should be noted that the cone angle is calculated taking into account only the spray cone formed between the spray outlet and 60% of the penetration length [28].

In Figure-17, we have plotted the curves of the cone angle upon time for two injection pressures. We performed the calculation for each case by changing the density of the ambient air ($\rho_a = 15\ \mathrm{kg.m^{-3}}$, $\rho_a = 25\ \mathrm{kg.m^{-3}}$, $\rho_a = 35\ \mathrm{kg.m^{-3}}$). The simulation curves show that, as the ambient air density increases, the cone angle increases for both injection pressures. We can also see that the injection pressure has little impact on the cone angle. This last result is in agreement with that of Naber [30].

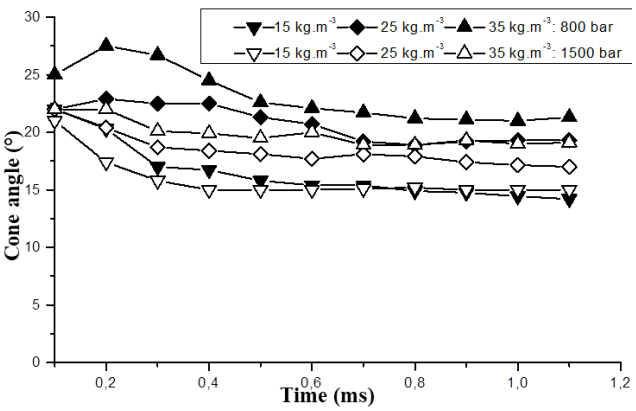


**Figure-17.** Cone angle upon time.

For each cone angle curve in Figure-17, we can notice that the cone angle is unstable at the beginning of the injection. But, after a certain time ($t \cong 0.45$ ms), the cone angle retains a constant value. This last result has been demonstrated by many research studies. In our case, and for the injection conditions mentioned above, the approximate correlation for the steady-state cone angle is: (see Figures 18 and 19)

$$\tan(\theta) \cong 0.7 \left(\frac{\rho_g}{\rho_l}\right)^{0.43}$$

It is similar to many correlations, the closest of which is that of Reitz [31]:

$$\tan(\theta) \cong 0.7 \left(\frac{\rho_g}{\rho_l}\right)^{0.5}$$

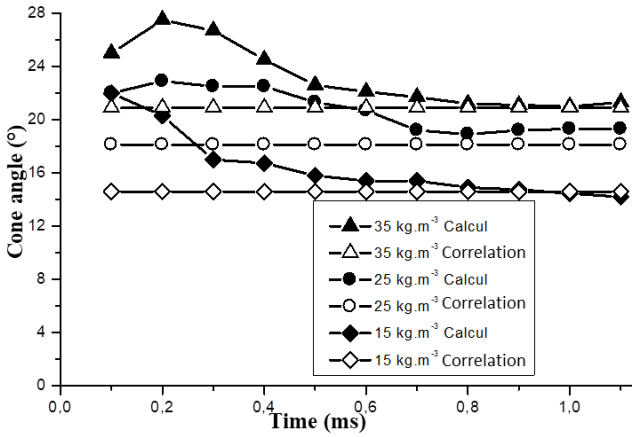


**Figure-18.** Evolution of the cone angle: $P_i = 800$ bar.

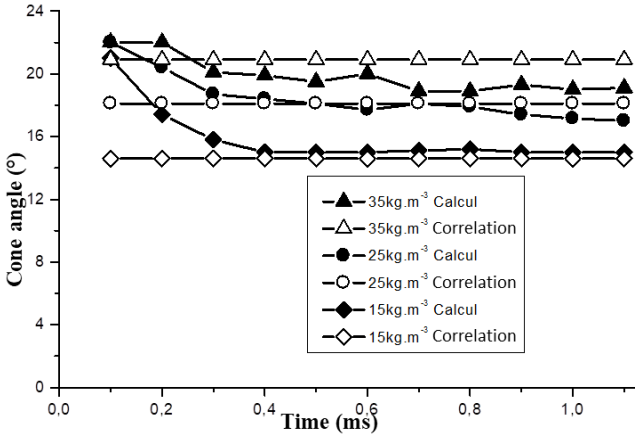


**Figure-19.** Cone angle evolution: $P_i = 1500$ bar.

### 5.5 The Effect of Turbulence Intensity at the Jet Exit

The intensity of turbulence at the injection nozzle outlet can be affected by the development of turbulence inside the diesel injector hole: the liquid flows at high velocity in high-pressure injectors (Common Rail), which means that the Reynolds number is very high. This results in a turbulent flow regime; the ratio (orifice length/nozzle diameter) and the cavitation phenomenon that occurs inside the injector hole, can give rise to fully developed turbulence at the outlet of the liquid injection nozzle. So, we can say that the turbulent intensity and discharge coefficient we took into account when establishing the velocity profile at the jet outlet to make the simulation calculations can include the physical phenomena that develop inside the diesel injector. For this reason, we are going to study the effect of turbulent intensity at the jet outlet on the characteristic variables of the diesel spray.

#### 5.5.1 Penetration length

In Figure-20, we plot the evolution of penetration length as a function of time after injection for two values of turbulence intensity at the jet outlet ($I = 1\%$ and $I = 10\%$). The curves show the effect of turbulence intensity at the jet exit on penetration length. When the time after injection is between $t = 0$ ms and $t = 0.3$ ms, the two curves coincide. After $t = 0.3$ ms, we can see a decrease in penetration length for $I = 10\%$ compared with $I = 1\%$. We can therefore deduce that as intensity increases, penetration decreases. This last result can be explained by the fact that turbulence influences the deformation of the liquid-air interface, which increases aerodynamic effects, further blocking jet penetration.

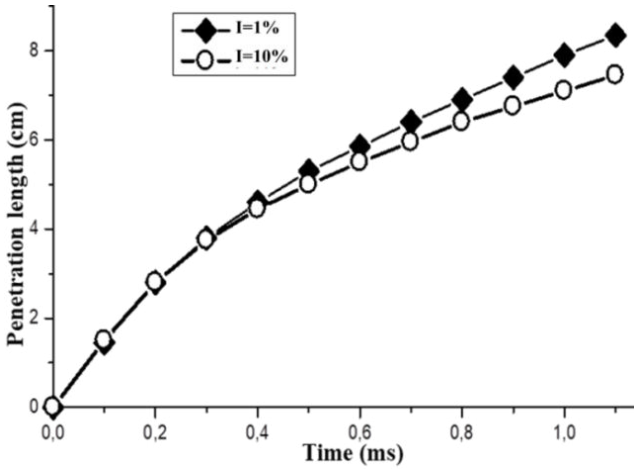


**Figure-20.** Penetration length upon time: $P_i = 150$MPa , $\rho_a = 25\ \text{kg.m}^{-3}$.

#### 5.5.2 Cone angle

In Figure-21, we plot the evolution of the spray cone angle upon time after injection for four values of turbulence intensity at the jet outlet ($I = 1\%$, $I = 10\%$, $I = 20\%$ and $I = 30\%$). The simulation curves show a negligible effect of turbulence intensity on the spray cone angle.

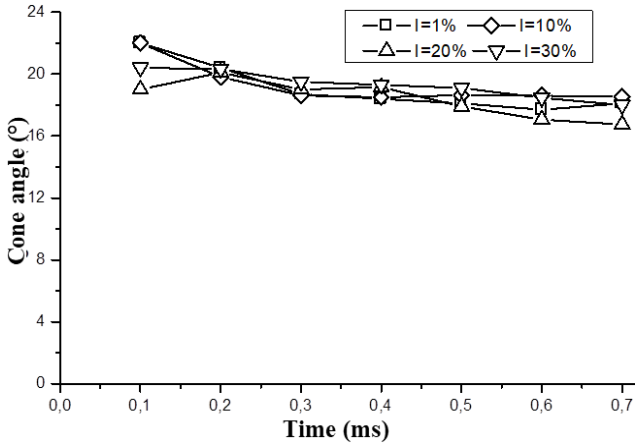


**Figure-21.** Spray cone angle upon time: $P_i = 150\text{MPa}$, $\rho_a = 25\ \text{kg.m}^{-3}$.

### 5.6 The Effect of Nozzle Diameter on Diesel Spray Evolution

Generally, technological developments in diesel injection always tend to increase injection pressure and reduce the diameter of the injector nozzle to ensure good atomization of the diesel spray in the combustion chamber. As a result, we have made calculations for diameters below $d = 0.2$ mm for high-pressure sprays.

In this section, we present the results of our calculations on the effect of injection diameter on diesel spray evolution. For the injection conditions, we referred to the article by Martinez-Martinez *et al* [25], choosing the outlet velocity corresponding to the injection pressure ($P_i = 130\text{MPa}$) for three injection nozzle diameters ($d = 0.13$ mm, $d = 0.17$ mm, $d = 0.2$mm). In this respect, we'll look at the effect of this geometric parameter on penetration length and potential core.

#### 5.6.1 Penetration length

In Figure-22, we have plotted penetration length upon time for three diameters ($d = 0{,}13$ mm, $d = 0{,}17$ mm, $d = 0{,}2$ mm) for $P_i = 1300$ bar. The simulation curves show that as we reduce the diameter of the injection nozzle, penetration also decreases.

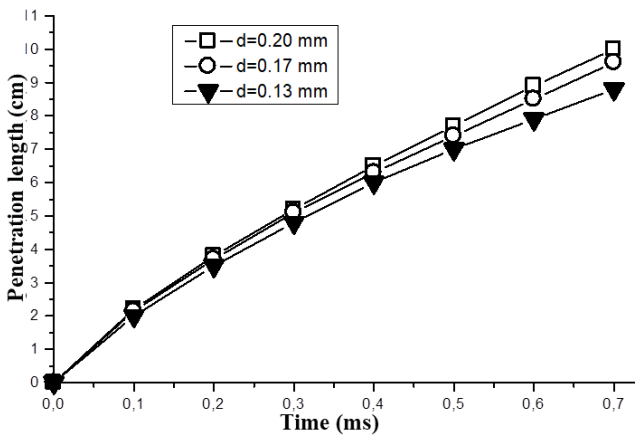


**Figure-22.** Penetration length upon time; $P_i = 130\text{MPa}$.

#### 5.6.2 Potential core

In this section, we'll study the impact of injection nozzle diameter on the potential core, using the two physical quantities that define this zone of the jet: the liquid volume fraction and the average velocity along the jet axis.

**Liquid volume fraction**

In Figure-23, we have plotted the liquid volume fraction along the spray axis for three injection nozzle diameters ($d_1 = 0.13$ mm, $d_2 = 0.17$ mm, $d_3 = 0.2$ mm). The injection pressure used is $P_i = 130\text{MPa}$.

Assuming that if the volume fraction of the liquid $\alpha_l > 0{,}9$ in a given zone, we can say that this zone is very dense. From this, we can deduce from the three graphs that as the diameter of the injection nozzle increases, the length of the dense zone becomes greater. This is one reason why engine manufacturers always try to minimise this diameter to avoid the liquid reaching the wall, leading to incomplete combustion.

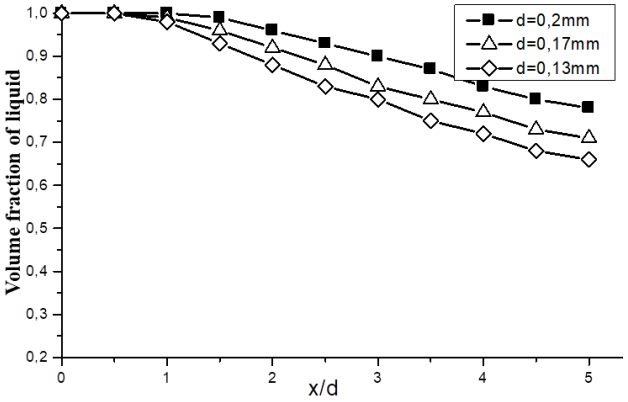


**Figure-23.** Liquid volume fraction at $t = 0.6$ ms in $y = 0$.

**The average velocity of the mixture**

In Figure-24, we have plotted the curve representing the axial evolution, on the jet axis, of the average velocity of the mixture for the three diameters.

We can see from the curves corresponding to diameters $d = 0.17$ mm and $d = 0.2$ mm that the average velocity remains constant up to $x = 10\ d$. This means that the length of the potential core is proportional to the injection nozzle diameters by a coefficient of ten. For diameter $d = 0.13$ mm, the zone where the average velocity remains constant does not exist.

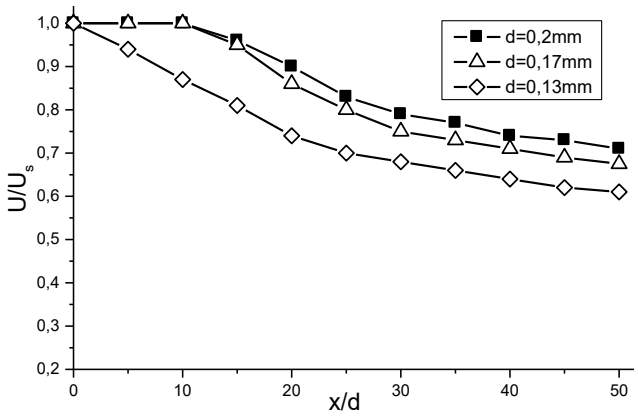


**Figure-24.** Evolution of the average velocity along the jet axis at $t = 0.6$ ms.

### 5.6.3 Cone angle

Figure-25 shows the effect of injection diameter on the cone angle for an injection pressure $P_i = 130$MPa. The simulation curves show a negligible effect of the injection diameter on the spray cone angle.

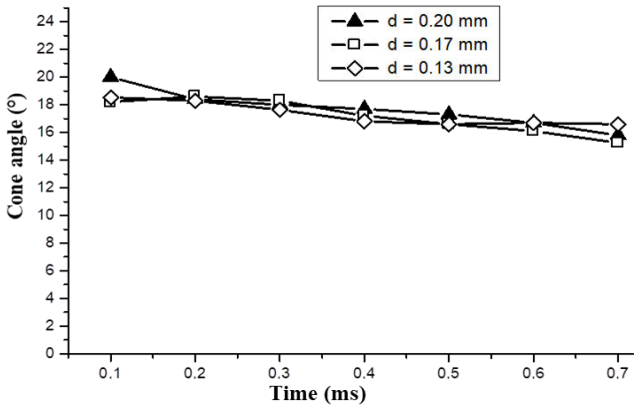


**Figure-25.** Cone angle upon time: $P_i = 130$MPa ; $\rho_a = 25\ \mathrm{kg.m^{-3}}$.

## 6. CONCLUSIONS

In the present article, we studied the dynamic behavior of a diesel jet at high injection pressure using two-dimensional geometry by numerical simulation. The results obtained have contributed to a better understanding of the phenomena governing the evolution of diesel sprays in the combustion chamber of a diesel engine. The simulation was carried out using averaged Navier-Stokes equations. The non-linear component in the averaged momentum equations (Reynolds stress term) was modelled using several turbulence models. Two-phase modelling was carried out using a VOF method and its coupling with the Level-Set method. The turbulence model that gave us results according to the literature was the k-$k_L$-ω model. However, the RSM model remains close. For the VOF and CLSVOF two-phase models, we found no difference between these two approaches.

A sensitivity study to mesh size, space-time numerical schemes, and coupling algorithms between pressure and velocity was carried out in this work.

The computational results of simulations made using the k-$k_L$-ω and VOF models enabled us to draw the following conclusions:

- Increasing injection pressure leads to faster penetration;
- For a given injection pressure, increasing ambient gas density delays spray penetration;
- The impact of ambient pressure becomes very important when the injection time exceeds a certain limit, which we call: transition time, from an evolution close to √t to an evolution close to t;
- Spray cone angle increases with ambient density and nozzle diameter;
- Spray cone angle does not depend on injection pressure or injection nozzle diameter;
- The volume fraction field near the injection nozzle and the average velocity along the jet axis indicate the existence of a potential core;
- The length of the potential core depends on the injection diameter. It increases as the diameter of the injection nozzle increases;
- The impact of turbulence intensity at the injection nozzle outlet on the cone angle is negligible. On the other hand, it does have a slight effect on penetration length: as intensity increases, penetration length decreases.

## REFERENCES

[1] A. Torregrosa *et al*. 2013. Sensitivity of combustion noise and NOx and soot emissions to pilot injection in PCCI Diesel engines. Appl. Energy.

[2] Yijie Wei *et al*. 2022. Measurement and modeling of the near-nozzle ambient gas entrainment of high-pressure diesel sprays. Fuel. 310: Part B, 15 February.

[3] J. Zhu *et al*. 2022. Simultaneous PIV/LIF-PIV measurements and numerical simulation of liquid flow and ambient gas flow for transient diesel spray. Fuel. 309: 1 February.

[4] Yijie Wei *et al*. 2020. Time-resolved measurement of the near-nozzle air entrainment of high-pressure diesel sprays by high-speed micro-PTV technique. Fuel. 268: 15 May.

[5] Yunpeng Wei *et al*. 2022. Experimental investigations into the effects of string cavitation on diesel nozzle internal flow and near field spray dynamics under different injection control strategies. Fuel. 309: 1 February.

[6] T. Ménard *et al*. 2006. Numerical jet atomisation. Part I: DNS simulation of primary breakup. Proceedings of ASME FEDSM, Miami.

[7] F. J. Salvador *et al*. 2016. Numerical simulation of primary atomization in diesel spray at low injection pressure. Journal of Computational and Applied Mathematics. 291: 94-102.

[8] M. Ghiji *et al*. 2017. Analysis of diesel spray dynamics using a compressible Eulerian/VOF/LES model and microscopic shadowgraphy. Fuel. 188: 352-366.

[9] G. Hindi *et al*. 2018. Effect of mesh refinement and model parameters on LES simulation of diesel sprays. International Journal of Heat and Fluid Flow. 71: 246-259.

[10] J. Brulatout *et al*. 2020. Interaction between a diesel-fuel spray and entrained air with single- and double-injection strategies using large eddy simulations. Propulsion and Power Research. 9(1): 37-50.

[11] Fatemeh Salehi *et al*. 2020. Large eddy simulation of high-pressure spray with a focus on injection pressure. International Journal of Heat and Fluid Flow. 82: 108551.

[12] P. Spalart et al. 1992. A one-equation turbulence model for aerodynamic flows.

[13] B. E. Launder *et al.* 1972. Lectures in Mathematical Models of Turbulence. Academic Press, London, England.

[14] S. A. Orszag *et al*. 1993. Renormalization Group Modeling and Turbulence Simulations. In International Conference on Near-Wall Turbulent Flows, Tempe, Arizona.

[15] H. Shih *et al.* 1995. A New Eddy-Viscosity Model for High Reynolds Number Turbulent Flows - Model Development and Validation. Computers Fluids. 24(%13): 227-238.

[16] D. C. Wilcox. 1998. Turbulence Modeling for CFD. DCW Industries, Inc. La Canada, California.

[17] F. R. Menter. 1994. Two-Equation Eddy-Viscosity Turbulence Models for Engineering Applications. AIAA Journal. 32(%18): 1598-1605.

[18] F. Menter *et al*. 2010. The Scale-Adaptive Simulation Method for Unsteady Turbulent Flow Predictions. Part 1: Theory and Model Description. Journal Flow Turbulence and Combustion. 85: 113-138.

[19] D. K. Walters *et al*. 2008. A three-equation eddy-viscosity model for Reynolds-averaged Navier-Stokes simulations of transitional flow. J. Fluids Eng. 130: 1-14.

[20] B. E. Launder *et al*. 1975. Progress in the development of a Reynolds-Stress Turbulence Closure. J. Fluid Mech. 68: 537-566.

[21] B. E. Launder. 1989. Second-Moment Closure: Present... and Future. Inter. J. Heat Fluid Flow. 10(%14): 282-300.

[22] D. Verhoven *et al*. 1998. Macroscopic and ignition characteristics of high-pressure sprays of single-component fuels. SAE 981069.

[23] L. Martinez. 2009. Simulation aux grandes échelles de l'injection de carburant liquide dans les moteurs à combustion interne. Thèse soutenue le 15 septembre.

[24] P. A. Beau. 2006. Modélisation de l'atomisation d'un jet liquide Application aux sprays Diesel. Thèse soutenue en.

[25] S. Martinez-Martinez *et al*. 2008. Liquid penetration length in direct diesel fuel injection. Applied Thermal Engineering 28.

[26] L. Souinida *et al*. 2015. The differentiation between the turbulence and two-phase models to characterize a Diesel spray at high injection pressure. American Journal of Engineering Research.

[27] H. Takahashi, H. Yanagisawa, S. Shiga, T. Karasawa et H. Nakamura. 1997. Analysis of High-Pressure Diesel Spray Formation in the early stage of Injection. Atomisation and Sprays. 7: 33-42.

[28] A. Doudou. 2007. Etude macro/microscopique des spray Diesel injectés par le système Common Rail avec la technique d'ombroscopie et l'anémomètre phase Doppler.

[29] J. V. Pastor, J. Arrègle, A. Palomares. 2001. Diesel Spray Image Segmentation with a Likelihood Ratio Test Applied Optics.

[30] J. Naber *et al*. 1996. Effect of Gas Density and Vaporization on Penetration and Dispersion of Diesel Sprays. SAE 960034.

[31] R. D. Reitz. 1978. Atomization and other break-up regimes of a liquid jet.